nature astronomy

Article

https://doi.org/10.1038/s41550-025-02486-x

Quantification of broadband chromatic drifts in Fabry–Pérot resonators for exoplanet science

Received: 24 April 2024

Accepted: 17 January 2025

Published online: 26 February 2025

Check for updates

Molly Kate Kreider[1,2,3], **Connor Fredrick**[1,2,3], **Scott A. Diddams**[1,2,3], **Ryan C. Terrien**[4], **Suvrath Mahadevan**[5,6,7], **Joe P. Ninan**[8], **Samuel Halverson**[9], **Chad F. Bender**[10], **Fred Hearty**[5,7], **Daniel Mitchell**[11], **Jayadev Rajagopal**[12], **Arpita Roy**[13], **Christian Schwab**[14] & **Jason T. Wright**[5,7,15]

Finding an Earth–Sun analogue is one of the longest-standing goals in astronomy. The detection of such a system using the radial velocity (RV) technique is highly challenging, and would require coordinated advances in astronomical telescopes, fibre optics, precision spectrographs, large-format detector arrays and data processing. Measurements at the necessary 10^{-10} level over multiyear periods would also require a highly precise calibrator. Here we explore simple and robust white-light-illuminated Fabry–Pérot (FP) etalons as spectral calibrators for precise RV measurements. We track the frequencies of up to 13,000 FP modes against laser frequency combs at two state-of-the-art spectrographs and trace unexpected chromatic variations of the modes to subpicometre changes in the dielectric layers of the broad-bandwidth FP mirrors, corresponding to a RV precision at the centimetres per second level. These results represent critical progress in precision RV measurements in two ways—they validate FP etalons as a more powerful stand-alone calibration tool and demonstrate the capability of laser frequency combs to extend RV measurement precision at the centimetres per second level over periods approaching a year. These advances highlight a path to achieving spectroscopic calibration at levels that will be critical for finding Earths like our own.

The discovery and characterization of an Earth-mass planet orbiting a Sun-like star at 1 au (aka Earth 2.0) is a long-standing challenge in astrophysics—with profound implications regarding the uniqueness of Earth, the formation of planetary systems and the conditions under which life could exist elsewhere in the Universe. Tremendous effort has been focused on this problem, with the dominant techniques of planetary transits and radial velocity (RV) measurements being used in tandem[1]. While a transit, or passage across the stellar disk, provides information on the size of an exoplanet, measurements of the stellar RV provide information on the mass of the exoplanet through the periodic Doppler shifts of the stellar spectrum (Fig. 1a,b). However, the RV detection of an Earth analogue requires Doppler precision of a few centimetres per second (fractionally 10^{-10}), which must be maintained over timescales of multiple years. Such a detection could then be followed by spectroscopic measurements made by instruments like the James Webb Space Telescope or the ANDES spectrograph at the Extremely Large Telescope to identify biomarkers in the atmosphere[2].

This is an extremely challenging and multifaceted measurement that will require simultaneous advances along multiple fronts[3]. At present, some of the most important outstanding challenges are a result of stellar surface activity and variable telluric contamination from our own atmosphere, both of which look like 'noise' and mask the

A full list of affiliations appears at the end of the paper. e-mail: mollykate.kreider@colorado.edu; scott.diddams@colorado.edu

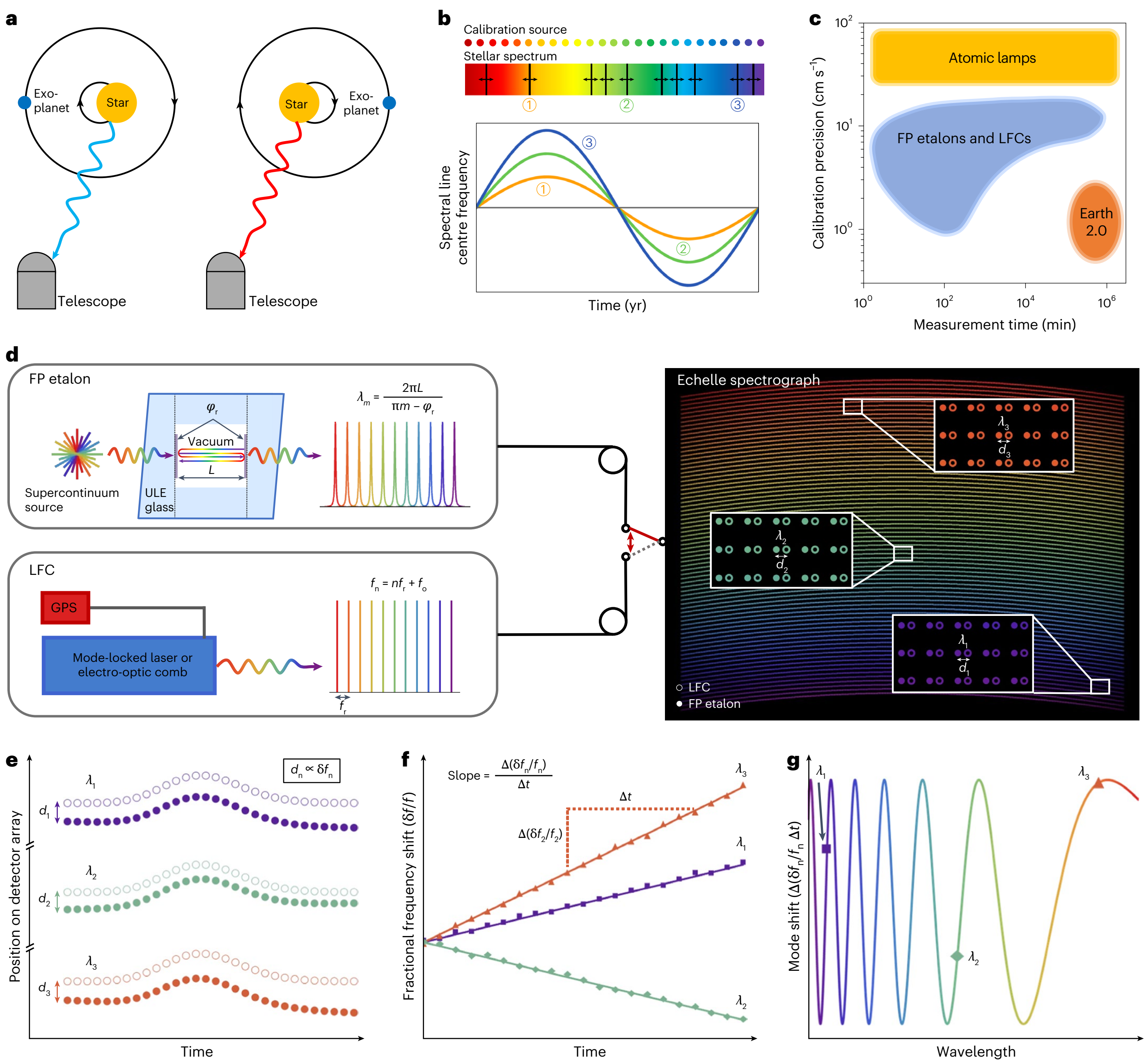

Fig. 1 | Introduction to etalon drift measurement. **a**, Principle of using RV measurements to detect exoplanets. **b**, A known calibration source is used to measure the periodic Doppler shift of absorption features in a stellar spectrum due to the gravitational pull of an exoplanet. **c**, Calibration precision levels needed to detect an Earth–Sun analogue (Earth 2.0) and the precision levels demonstrated by several different classes of calibrator. **d**, Experimental set-up of chromatic drift measurements on the Habitable-zone Planet Finder (HPF) and NEID etalons, as detailed in ref. 14. An echelle spectrograph is alternately illuminated by LFC (where f_r is the repetition rate, f_o is the carrier envelope offset frequency and f_n is the frequency of the nth mode) and etalon light (here m is an integer, φ_r is the reflective mirror phase shift, L is the cavity length and λ is wavelength. ULE, ultra-low-expansion). **e**, The spatial location (that is, frequency) of each mode drifts over time, as illustrated for three modes. **f**, The drift of the frequency comb is indicative of instrument drift, and the change in spacing between a frequency comb–etalon mode pair, $\Delta(\delta f_n)$, is indicative of the etalon drift. The fractional frequency shift for any given mode is linear in time. **g**, The slopes of the fractional frequency shift can be plotted across the wavelength range of interest, showing the complicated chromatic drift of the etalon[14].

desired centre-of-mass RV Doppler shift, as well as increase the time and effort it takes to realize long-term measurement cadences with sufficient photon signal-to-noise ratios[4,5]. Stable spectrographs and the precise spectrograph calibration that provide the stable reference against which tiny Doppler shifts are measured are equally important. Conventional sources for calibration include atomic emission lamps and gas absorption cells, both of which have intrinsic limitations in uniformity and unknown long-term stabilities that hinder their precision[6].

Laser frequency combs (LFCs) provide a broad spectral array of discrete and evenly spaced emission lines that can be fully stabilized to absolute frequency standards[7]. These properties make LFCs a near ideal spectrograph calibration source[8,9], and in recent years, they have shown fractional calibration precisions below 10^{-10} (refs. 10,11). However, they lack full spectral coverage in the blue region of the spectrum. Moreover, their implementation remains costly and complex, and is therefore limited to a few RV instruments situated at premier facilities. No calibration technique (frequency combs included) has yet demonstrated the capability to resolve 1 cm s^{-1} Doppler shifts over timescales of years or longer. As summarized in Fig. 1c, there is a gap between the experimentally demonstrated timescales over which etalon and LFC-calibrated spectrographs have achieved this precision level and the necessary timescales to detect an Earth–Sun analogue.

Our work addresses this issue by exploring new capabilities and resolving systematic uncertainties in broadband, white-light illuminated Fabry–Pérot (FP) etalons, which have long been used in astronomical spectroscopy[12]. They are used as primary calibrators (in combination with lamps) in some spectrographs (for example, ref. 13), and in others extend the overall spectral coverage to blue wavelengths not easily achieved with LFCs, but they lack long-term absolute stability.

We investigate this shortcoming by analysing and modelling two extended (up to 6 month) cross-calibration studies that resolve puzzling chromatic drifts that have appeared in multiple installed FP etalons[14]. Specifically, we show that, with the help of an LFC, it is possible to track and characterize ~13,000 modes of an FP etalon with a precision that translates to subpicometre resolution of the optical length of the FP etalon. When combined with careful modelling of relaxation in the dielectric coating of the FP etalon mirrors, we can disentangle drifts consistent with an achromatic change in cavity length versus higher-order drifts with equivalent RV residuals at a level near 3 mm s^{-1} (10^{-11}). This new understanding of the complicated drifts of broad-bandwidth FP cavities can inform future mirror design parameters and immediately improve the achievable precision level when using them as stand-alone calibrators that are periodically referenced to absolute frequency standards.

Results

Measuring chromatic mode drift in FP etalons with LFCs

Within the landscape of calibration sources, FP etalons are particularly attractive due to their unique combination of high spectral resolution and information content, similar to that of an LFC[15], but with relative simplicity and cost efficiency. They have become increasingly commonplace in high-precision RV spectrographs and are used as calibrators in a number of major instruments at large telescopes, including the Calar Alto high-Resolution search for M dwarfs with Exoearths with Near-infrared and optical Échelle Spectrographs (CARMENES)[16], the Echelle SPectrograph for Rocky Exoplanets and Stable Spectroscopic Observations (ESPRESSO)[17], the High Accuracy Radial velocity Planet Searcher (HARPS)[18], HPF[6], the Keck Planet Finder (KPF)[19], the M-dwarf Advanced Radial velocity Observer Of Neighboring eXoplanets (MAROON-X)[20], NEID[21], the Near Infra Red Planet Searcher (NIRPS)[22] and the SPectropolarimètre InfraROUge (SPIRou)[23]. They are also slated to be implemented in new instruments to be installed at large telescopes, including iLocator[24] and the GMT-Consortium Large Earth Finder (G-CLEF)[25].

While mode locking fixes the line spacing of an LFC, the modes of an FP cavity are determined by the local resonance condition, which is subject to the wavelength-dependent optical path length of the cavity geometry and mirror coatings. The stability of its spectra is tied to the stability of the cavity's mechanical and optical properties, which can drift with time. Ultra-stable etalons that exhibit a minimal amount of drift have been developed for precision spectroscopy and optical clocks[26]. Single-frequency near-infrared lasers locked to the modes of silicon resonators held at cryogenic temperatures at a zero crossing of the coefficient of thermal expansion have demonstrated drift rates below one part in 10^{-13} per day[27,28]. While not as high-performing as those designed for cryogenic temperatures, cavities built using room-temperature ultra-low expansion materials operate in the visible region of the spectrum. Such cavities are still capable of achieving fractional stabilities at 10^{-11} from day to day (equivalent to a frequency drift of ~0.1 Hz s^{-1} at 1 μm)[29–31] and are particularly attractive for astronomical spectroscopy.

One method of circumventing limitations due to drift is to continuously reference one mode of an etalon to an absolute frequency standard, such as an atomic transition, and then extrapolate the behaviour of that single mode to the behaviour of the etalon's entire spectrum[32–34]. However, this technique is only capable of correcting drift in an etalon to the level at which the drift behaviour is achromatic, as it implicitly assumes that a fractional change in cavity length $\Delta L/L$ is equal to the fractional frequency change $\Delta f/f$ of any cavity mode. This model describes the gradual relaxation of the etalon spacer[35], which is well documented[36].

However, measurements made at several etalon systems employed in precision RV instruments have shown that etalon mode drift can be substantially and unexpectedly more complex[14,17,37]. Using LFCs, we have made comprehensive and long-term measurements of the etalons used with the HPF and NEID spectrographs. The unique broadband nature of these studies, which measure the average daily drift rate of up to approximately 13,000 modes (or hundreds of nanometres) of the two FP etalons, is made possible by leveraging the instrument architecture necessary for high-precision RV detection.

A simplified schematic of the etalon characterization is presented in Fig. 1d, with an intuitive illustration of the measurement results in Fig. 1e–g. An echelle spectrograph (for example, HPF or NEID) is alternately illuminated by the light from a fully stabilized LFC and the temperature-stabilized vacuum-held ultra-low-expansion etalon[14,37]. The wavelengths of the LFC and etalon modes are mapped to relative spatial positions on the spectrograph detector array, where they are monitored over time (as shown in Fig. 1e). Common drift of the LFC and etalon modes is indicative of spectrograph drift, but it is the change in the relative offset between the etalon modes and the wavelength solution from the stable LFC modes that reveals the etalon mode drift. The fractional frequency mode drift of the etalon may be linear in time, but the specific slope of the drift varies from one spectral region to another (Fig. 1f). Plotting the slope of the drift of etalon modes in a spectral region gives the drift shown in Fig. 1g.

Such oscillatory behaviour has been verified for both the NEID and HPF spectrographs, and qualitatively analogous behaviour has been found for the etalon system of the ESPRESSO[17] spectrograph. Surprisingly, it implies that the optical length of the etalon is effectively increasing and decreasing in different wavelength regions. This poses a clear problem for high-precision RV spectrograph calibration, as such etalon mode drifts are undetectable and thus unaccounted for. This drift behaviour also raises important considerations for experiments that use multiple FP cavity modes for frequency referencing in precision spectroscopy[38–42], particularly when those modes have large spectral separation.

The role of multilayer coatings in FP drifts

Previous work has speculated that the wavelength-dependent behaviour may stem from the mirror coatings[14,37], which are built on complex optical interferences arising from alternating layers of dielectric materials. Other work has attempted to benchmark possible drift behaviour due to mirror phase drifts[43], but has not been conclusive. Here we have identified the source of the observed chromatic drift behaviour in the mirror coatings of the HPF and NEID etalon systems and succeeded in developing a physical model for this drift.

Through our modelling, we determined that the gradual expansion of the outermost layers of the mirror coating causes a mode shift that is consistent with the measured HPF and NEID etalon drifts. In particular, we show that the drift behaviour of the HPF and NEID etalons can be tied to an ~100×10^{-15} m (100 fm) change in the outer layers of the two mirrors.

An FP etalon, as pictured in Fig. 2a and illustrated schematically in Fig. 2b, transmits a mode spectrum determined by the resonance condition, which ensures that resonant modes occur at wavelengths where the round-trip phase shift of the light in the cavity is equal to an

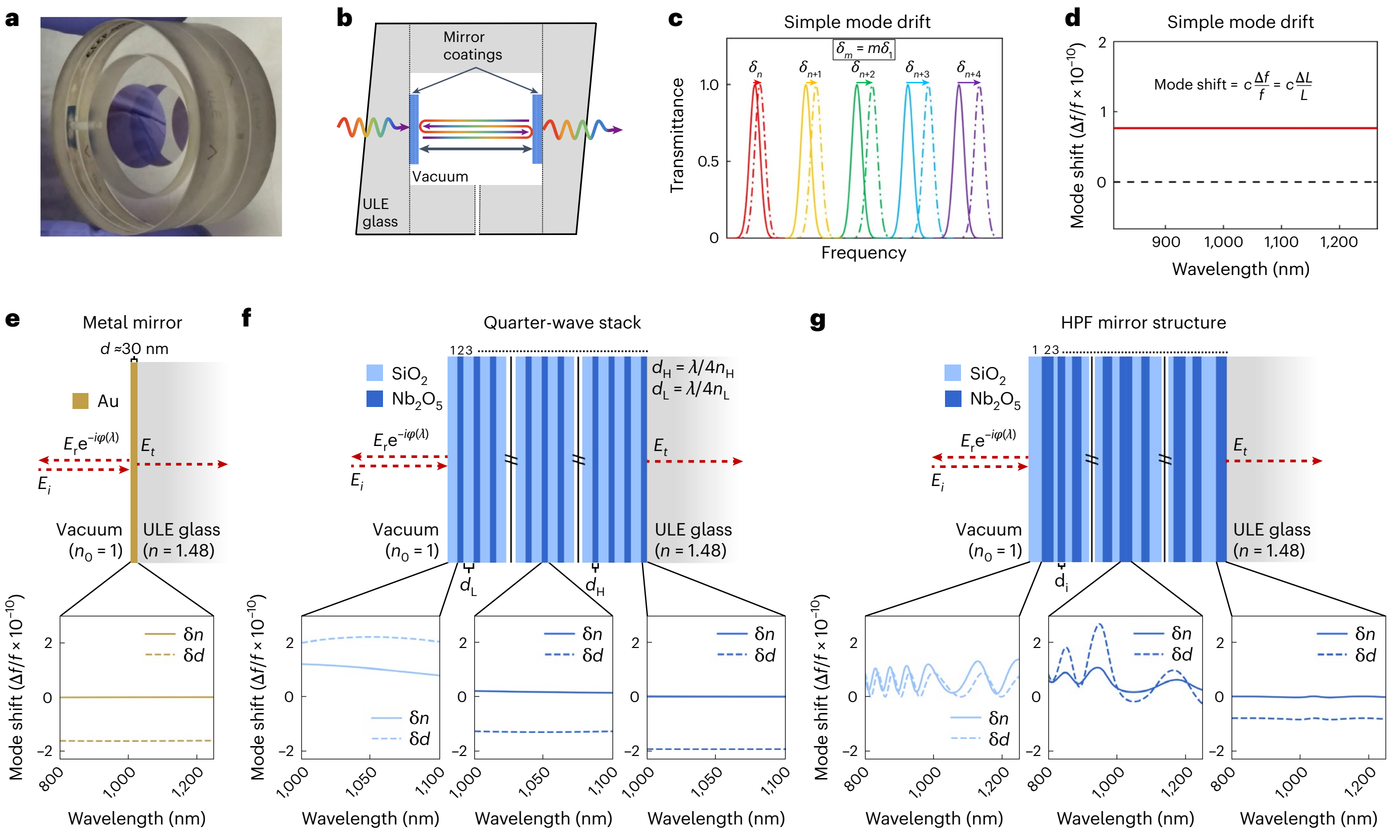

Fig. 2 | Etalon mirror coatings. a,**b**, Photograph (**a**) and schematic (**b**) of an FP etalon. **c**,**d**, The simplest drift mechanism in an FP etalon is a change in L, which results in the mode frequency drift illustrated conceptually in **c**, corresponding to the constant, fractional drift behaviour shown **d**. **e**,**f**, More complicated drift behaviour results from changes in three mirror structures with 92% reflectivity: the modelled drift resulting from a refractive index ($\delta_n = +10^{-6}$) and layer thickness ($\delta_d = +5 \times 10^{-4}$ nm) change for a thin metal mirror (**e**) and the top, middle and bottom layers of a quarter-wave stack (**f**), respectively. **g**, Markedly more complex modelled drift results from refractive index ($\delta_n = +10^{-6}$) and layer thickness ($\delta_d = +5 \times 10^{-4}$ nm) changes in the first, sixteenth and thirty-fourth layer of the HPF mirror structure. In **e**–**g**, E_i, E_r and E_t represent the incident, reflected and transmitted electric fields, respectively; n_H and n_L represent the high and low index of refraction, and d_H and d_L represent the high and low layer thickness, respectively.

integer multiple of 2π. For an etalon in a vacuum, this condition yields modes with frequencies given as:

$$f_m = \frac{c}{2L}(m - \varphi_r/\pi). \qquad (1)$$

where c is the velocity of light, m is an integer and φ_r is the reflective mirror phase shift, which is generally dependent on wavelength but is assumed to be the same for both mirrors of the etalon.

It is instructive to consider potential sources of mode drift through this resonance condition, as both L and $\varphi_r(\lambda)$ represent physical properties of the cavity that may change over time. The simplest mode drift behaviour would stem from a gradual drift in L, over time, which produces a simple, predictable drift rate across the mode spectrum ($\Delta f/f \propto \Delta L/L$).

In contrast, φ_r intrinsically varies with wavelength in a complicated manner, and we discuss the details of calculating this term (and include plots of φ_r for NEID and HPF) in Supplementary Note 1. We investigate the impact of various physical perturbations on the coating structure by modelling the shift in f_m using established matrix techniques to determine φ_r (ref. 44). With knowledge of φ_r, we first used a numerical solver to determine a base mode spectrum from equation (1). We then recalculated the mode spectrum using the slightly perturbed φ_r to determine the difference between the new and original mode locations across the wavelength spectrum of interest in units of fractional frequency, $\Delta f/f$.

Figure 2e–g illustrates characteristic modelling results for three different types of mirror coating with approximate reflectivities of 92%, which correspond to that of the mirrors deployed in the HPF and NEID cavities. In each case, individual layers in the coating structure were perturbed by identical changes in their refractive index ($\delta_n = +10^{-6}$) and layer thickness ($\delta_d = +5 \times 10^{-4}$ nm), which were chosen because these perturbations result in mode shifts that are similar in scale to the measured daily drift of the HPF etalon.

Figure 2e illustrates mode drift for the simplest possible mirror: a thin layer of metal. As one may expect given the relative simplicity of a single layer, perturbing a 30 nm gold layer produced minimal drift across the wavelength spectrum. Unfortunately, these mirrors are in general not suitable for cavities deployed for astronomical applications due to the metal's absorption and resulting low transmission on resonance.

Figure 2f illustrates mode drift for a simple quarter-wave stack comprising alternating layers of silica and niobia. The reflected phase from a quarter-wave stack is fairly simple, and this simplicity means that perturbations to the coating structure do not give rise to the chromatic drift observed in the HPF and NEID etalons. However, such mirrors are generally unsuitable for spectrographs like HPF and NEID, as they do not have a flat reflectivity spectrum across a sufficiently broad bandwidth.

The mirror coatings used in the HPF and NEID etalons are deposited via magnetron sputtering and comprise alternating layers of silica and niobia, with the outermost or first layer (that is, the layer closest

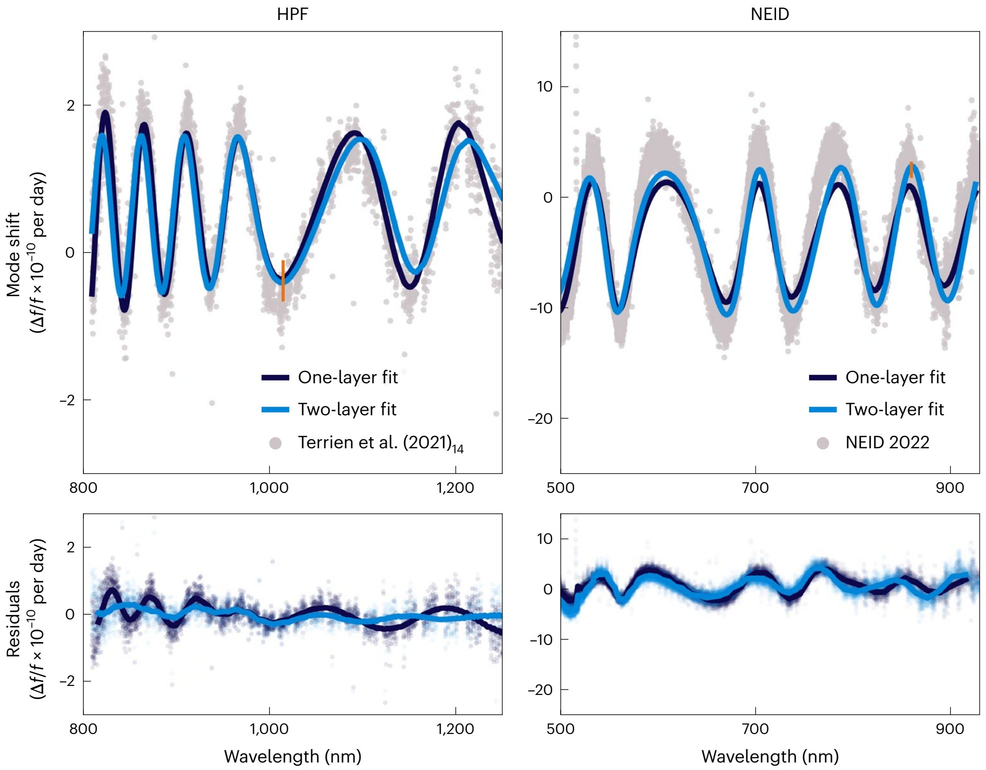

Fig. 3 | Fits to the drift data. Top: fits of the perturbative models to the measured HPF etalon data[14] (left) and NEID etalon data (right) with representative error bars for the raw data shown in orange ($\sigma_{\mathrm{HPF}} = 2.8 \times 10^{-11}$ and $\sigma_{\mathrm{NEID}} = 7.3 \times 10^{-11}$). Bottom: corresponding residuals of the model fits for both etalons, with lines corresponding to the moving averages. One- and two-layer fit parameters and values for HPF and NEID are listed in Tables 1 and 2.

to vacuum) being silica in both cases. They are substantially more complicated, as having a constant reflectivity curve across hundreds of nanometres of bandwidth requires large variations in layer thickness. A simple schematic of the drift is shown in Fig. 2g for the 34-layer HPF structure; the 48-layer NEID etalon exhibits qualitatively similar behaviour. We found that perturbations to individual layers of the mirror structure can be broken into regions with qualitatively similar behaviour, which we discuss in detail in Supplementary Note 2. This analysis showed us that the drift of the HPF and NEID mirrors depends primarily on the drift of the outermost layers.

Modelling chromatic mode drift in HPF and NEID FP etalons

A full analysis of the two etalons is presented in Fig. 3, which shows fits for changes to the outermost layer and the outermost two layers for the HPF and NEID etalons. These results were calculated as a linear combination of the effects of changes in individual layer thicknesses or refractive indices, as discussed in Supplementary Note 2. There were two fit parameters for each layer in a given model: the first for the refractive index and the second for the thickness change in each layer. We also included a fit parameter to account for the bulk offset due to gradual spacer relaxation. These fit values are reported in Tables 1 and 2. Although fitted independently and without constraints, the relative changes in the refractive index and layer thickness were consistent (within a factor of two) with simple models that couple refractive index to changes in density[45]. We do not include fits for higher layer numbers, as including more than the outermost two layers did not yield reasonable parameters when constrained to physically relevant orders of magnitude and relative sign.

Table 1 | HPF mirror drift fits

HPF fits	One layer	Two layers
Spacer shift	-7.6×10^{-11}	-1×10^{-10}
$\delta_{d,1}$ (nm d^{-1})	$+5.6\times10^{-4}$	$+8.2\times10^{-4}$
$\delta_{n,1}$ (d^{-1})	-1.5×10^{-6}	-3.8×10^{-6}
$\delta_{d,2}$ (nm d^{-1})	–	$+4.1\times10^{-4}$
$\delta_{n,2}$ (d^{-1})	–	-2.2×10^{-6}
Data r.m.s.	1.04×10^{-10}	1.04×10^{-10}
Residual r.m.s.	4.95×10^{-11}	3.71×10^{-11}

One- and two-layer fit values for the HPF data are presented, including the root mean square (r.m.s.) of the HPF drifts before fitting and the r.m.s. of the residuals of each fit. d, day. Subscripts denote the layer to which the change is made; for example, $\delta_{d,1}$ denotes a change to thickness in the first layer of the mirror.

The structure in the residuals of the one-layer HPF and NEID fits may be due to differences between the layer thicknesses input into the model and those that were actually manufactured. The one-layer HPF fit of Fig. 3 is slightly wavelength shifted from the measured data. Manufacturing tolerances are expected on the deposited layer thicknesses, and we found that randomly perturbing the entire structure shifted the relative wavelength position of the one-layer models. For this reason, while it is reasonable to conclude that changes in the first few mirror layers are the likely cause of the measured behaviour of the HPF and NEID etalons, fully determining the mechanism and drift rates would require further study of the exact physical properties of the mirror. Specifically, we anticipate that it will be important to have more accurate information on the refractive index and deposited thickness of each layer than we currently possess, which could also affect the quality of our fit.

While the primary drift mechanism of the HPF and NEID etalons can be explained by perturbations to the outermost layers of the mirror stack, we also conducted a thorough investigation of other physically reasonable drift mechanisms, including polarization and incident angle

Table 2 | NEID mirror drift fits

NEID fits	One layer	Two layers
Spacer shift	$+2.4\times10^{-10}$	$+5.6\times10^{-10}$
$\delta_{d,1}$ (nm d^{-1})	$+4\times10^{-3}$	$+4.7\times10^{-3}$
$\delta_{n,1}$ (d^{-1})	-1.4×10^{-4}	-1.8×10^{-5}
$\delta_{d,2}$ (nm d^{-1})	—	$+6.8\times10^{-4}$
$\delta_{n,2}$ (d^{-1})	—	-1.3×10^{-6}
Data r.m.s.	1.86×10^{-9}	1.86×10^{-9}
Residual r.m.s.	2.34×10^{-10}	2.18×10^{-10}

One- and two-layer fit values for the NEID data are presented, including the r.m.s. of the NEID drifts before fitting and the r.m.s. of the residuals of each fit.

changes, temperature changes and manufacturing tolerances. These modelling results are summarized and plotted in Supplementary Note 3. We concluded that none of these alternative mechanisms is responsible for the etalon drift measured by the HPF or NEID spectrographs, but might still be present in the HPF and NEID residuals or in other systems more generally.

Discussion

In summary, we modelled the effects of a number of mirror-coating-related causes for the chromatic mode drift in the HPF and NEID etalons, including incident angle variation, polarization fluctuation and temperature gradients. We were able to exclude the majority of these simple changes as the mechanism responsible for the HPF and NEID mode drifts. We also approached the modelling via a perturbative layer-by-layer analysis of the mirror coating stack, and found that changes in the first few layers of the mirror system cause mode shifts that agree with the observed HPF and NEID etalon behaviour.

The most likely mechanism for the wavelength-dependent mode shift is a gradual expansion of the outermost one or two layers of the mirror coating over time. A reasonable explanation for this behaviour comes from the fact that the magnetron-sputtered stacks have some level of intrinsic, compressive stress due to the deposition method[46]. The outermost layer of the structure faces a vacuum, which offers little resistance, meaning that this layer can gradually expand and relax (whereas other, deeper layers in the system are more constrained by the surrounding layers and substrate, which offer some resistance to such a process). This relaxation could produce refractive index and thickness changes that are consistent with the relative magnitude and sign of the parameters fitted by the models discussed above.

It is also possible that the drift behaviour could be explained by the deposition of some contaminant (for example, water) in the vacuum chamber on the mirror surfaces. The deposition of some other material on the mirror stack is effectively equivalent to a change in the outermost layer of the stack, so our model is unable to distinguish between the two. We also note that neither of these explanations applies to FP etalons with soft coatings (for example, ESPRESSO), as soft coatings are not compressive and are more prone to processes such as outgassing or water absorption.

Of course, we also note that etalon drift is one of many complex sources of instrumental drift, such as optical, thermo-mechanical and detector-driven effects, and further work will be necessary to determine the level of instrumental improvement resulting from calibrating the wavelength solution to account for etalon drift behaviour. We plan to carry out this investigation in the future using NEID data presented in this Article and data obtained more recently, and will attempt to integrate a chromatic correction directly into the wavelength module of the NEID pipeline. If successful, future studies reprocessing NEID archive data will be able to exploit these corrections.

The modelling results we present are by nature specific to the HPF and NEID etalons, and further analysis of other etalon systems will be necessary to determine the dominant effects of the coatings in each. However, they do provide clear evidence for etalon mirror coatings acting as the mechanism behind wavelength-dependent mode drift. As such, our work lays the foundation for additional modelling, mirror design and fabrication with the goal of identifying more stable mirror coatings for future etalon systems.

In the design of such etalon mirrors, it is typically only the bandwidth and reflectivity that are are optimized. With the addition of our insights and modelling, it should now be possible to impose additional constraints on the coating design. In particular, we note that the complexity of the mirror phase across the wavelength region of interest is directly tied to the etalon drift behaviour for HPF and NEID (specifically, in both cases, the drift behaviour is proportional to $\cos(\varphi_r)$). Therefore, constraining mirror designs to phases with smaller variations in $\cos(\varphi_r)$ across the spectrum should mean that, even for the drift mechanisms explored in this Article, the drift behaviour would be less complex. This would, in turn, make locking the cavity to a known reference more straightforward. In general, we expect opportunities to minimize the impact of coating structure, ageing and manufacturing tolerances to emerge in this largely unexplored high-dimensional design space to provide more stable and predictable etalon behaviour.

Finally, we note that the broadband and high experimental precision required to understand the drift mechanisms of FP etalons at the centimetres per second level and at timescales longer than 6 months is not dissimilar to the demands of extreme-precision RV measurements. Our work thus also separately provides a unique and critical validation of LFCs as astronomical calibrators, offering clear evidence that they are capable of performing at both the precision level and timescale that will be required for the detection of an Earth analogue. In seeking to understand, characterize and improve on one of our oldest calibration sources, we therefore simultaneously offer a crucial validation of our newest ones.

Methods

HPF and NEID are both stabilized, fibre-fed, cross-dispersed echelle spectrographs that are optimized for RV exoplanet detection. HPF, located at the Hobby–Eberly Telescope at McDonald Observatory in Texas, operates in the near-infrared (820–1,280 nm) at a spectral resolution ($\lambda/\Delta\lambda$) of approximately 55,000 (ref. 47). NEID, located at the WIYN telescope at the Kitt Peak Observatory in Arizona, operates at visible wavelengths (380–930 nm) at a spectral resolution of 110,000 (refs. 21,48,49). Both systems are equipped with a suite of calibration sources, including LFCs (which provide a reliable absolute calibration) and FP etalons, which are the devices of interest here. The LFC at HPF is a custom electro-optic frequency comb with nanophotonic spectral broadening[10], while the NEID comb is a commercial instrument (Menlosystems) based on a mode-locked laser and nonlinear optical fibre. Spectra of these sources are recorded daily, enabling long-term tracking of the relative, wavelength-resolved drift of their spectral features.

The FP system installed at HPF was described in detail in ref. 14. The FP system at NEID is similar to that at HPF. Planar dielectric mirrors manufactured by LightMachinery are attached to a 7.5 mm ultra-low-expansion spacer, and sit in a stabilized chamber designed by Stable Laser Systems. Light from an NKT SuperK Extreme supercontinuum source is coupled to the FP etalon via single-mode fibre (LMA-5 fibre from NKT). Finesse ($F > 30$) of the FP etalon is maintained across the NEID bandpass. This means that the mirrors need to maintain constant reflectivity across the covered bandwidth, motivating the many-layer mirror structure described above. This system delivers a mode spectrum of distinct, 20-GHz-spaced modes to NEID (or 30 GHz for HPF) that can be used for spectrograph calibration. These differences in mode spacing, as well as the differences in the frequency bandwidths covered (~130 THz for HPF and ~265 THz for NEID) lead to the differing numbers of modes studied (5,000 for HPF and 13,000 for NEID).

For this study, we examined multi-month FP etalon/LFC relative drift monitoring from both HPF and NEID. The HPF spectral dataset (spanning roughly 6 months, from November 2018 to May 2019), along with associated methods for measuring the mode centroids and data quality, are described in ref. 14. The same analysis pipeline was used to analyse spectra from the NEID FP system, and we briefly summarize its application to the NEID spectra here. We focused on ~1,000 FP spectra spanning 1 September 2021 to 1 March 2022, which we downloaded from the NEID archive (https://neid.ipac.caltech.edu/search.php). These spectra were obtained through the CAL fibre in HR mode. Spectra in the NEID archive are provided in wavelength-calibrated form by the standard NEID pipeline (v1.2.1), which uses the LFC in combination with the FP and hollow cathode lamps to map pixel index to wavelength. The NEID pipeline documentation describes the details of this process[50].

For this work, we focused on the wavelength range most reliably spanned by the LFC (5,100–9,300 Å), where the wavelength calibration is of the highest quality. This waveband contains more than 13,000 FP modes. Within this range, an independent pixel-to-wavelength mapping is defined for each spectral order of NEID. This mapping is parameterized as a ninth-order Legendre polynomial, which is refitted each day using spectra of the LFC. A low-order time-dependent correction is applied to this polynomial based on measurements of the FP spectrum throughout the day. Because the FP etalon is used only for finding these short-term corrections, the long-term behaviours of the FP etalon that we analysed here are not dependent on any assumptions about the FP etalon drift behaviour. Similarly to the wavelength calibration quality for HPF[14], the residual r.m.s. values for the polynomial fits are <10 m s^{-1}. There is some correlated structure at the level of a few metres per second across tens of modes, but this is at a much smaller scale than the long-term broadband drift behaviour of the FP etalon that we analysed.

As was done with the HPF dataset[14], we measured the wavelength centroid of each of the ~13,000 FP modes in the NEID spectra using a least-squares fit of a Gaussian function and tracked the motion of these centroids over time. Over the time span studied, the behaviour of the FP modes for both HPF and NEID is generally well described by a linear drift, so we quantified the wavelength-dependent drift using a least-squares fit of a line to the time series of centroids for each mode. Examples of these linear fits for the NEID data are shown in Supplementary Note 4.

Data availability

All data needed to reproduce the results of this Article are available at https://scholar.colorado.edu/concern/datasets/m326m3334 (ref. 51).

References

1. Lovis, C. et al. Radial velocity techniques for exoplanets. In *Exoplanets* (ed. Seager, S.) 27–53 (University of Arizona Press, 2010).
2. Palle, E. et al. Ground-breaking exoplanet science with the ANDES spectrograph at the ELT. Preprint at https://arxiv.org/abs/2311.17075 (2023).
3. Fischer, D. A. et al. State of the field: extreme precision radial velocities. *Publ. Astron. Soc. Pacif.* **128**, 066001 (2016).
4. Wang, S. X. et al. Characterizing and mitigating the impact of telluric absorption in precise radial velocities. *Astron. J.* **164**, 211 (2022).
5. Vanderburg, A. et al. Radial velocity planet detection biases at the stellar rotational period. *Mon. Not. R. Astron. Soc.* **459**, 3565–3573 (2016).
6. Mahadevan, S. et al. The Habitable-zone Planet Finder: a stabilized fiber-fed NIR Spectrograph for the Hobby-Eberly Telescope. *Proc. SPIE* **8446**, 84461S (2012).
7. Diddams, S. A., Vahala, K. & Udem, T. Optical frequency combs: coherently uniting the electromagnetic spectrum. *Science* **369**, eaay3676 (2020).
8. Murphy, M. T. et al. High-precision wavelength calibration of astronomical spectrographs with laser frequency combs. *Mon. Not. R. Astron. Soc.* **380**, 839–847 (2007).
9. McCracken, R. A., Charsley, J. M. & Reid, D. T. A decade of astrocombs: recent advances in frequency combs for astronomy [invited]. *Opt. Express* **25**, 15058–15078 (2017).
10. Metcalf, A. J. et al. Stellar spectroscopy in the near-infrared with a laser frequency comb. *Optica* **6**, 233–239 (2019).
11. Probst, R. A. et al. A crucial test for astronomical spectrograph calibration with frequency combs. *Nat. Astron.* **4**, 603–608 (2020).
12. Buisson, H., Fabry, C. & Bourget, H. An application of interference to the the study of the Orion Nebula. *Astrophys. J.* **40**, 241–258 (1914).
13. Schmidt, T. M. et al. Fundamental physics with ESPRESSO: towards an accurate wavelength calibration for a precision test of the fine-structure constant. *Astron. Astrophys.* **646**, A144 (2021).
14. Terrien, R. C. et al. Broadband stability of the Habitable Zone Planet Finder Fabry-Pérot etalon calibration system: evidence for chromatic variation. *Astron. J.* **161**, 252 (2021).
15. Halverson, S. et al. Development of fiber Fabry-Perot interferometers as stable near-infrared calibration sources for high resolution spectrographs. *Publ. Astron. Soc. Pacif.* **126**, 445 (2014).
16. Schäfer, S. et al. Two Fabry-Pérots and two calibration units for CARMENES. *Proc. SPIE* **10702**, 1070276 (2018).
17. Schmidt, T. M. et al. Chromatic drift of the espresso Fabry-Pérot etalon. *Astron. Astrophys.* **664**, A191 (2022).
18. Wildi, F., Pepe, F., Chazelas, B., Curto, G. L. & Lovis, C. A Fabry-Perot calibrator of the HARPS radial velocity spectrograph: performance report. *Proc. SPIE* **7735**, 77354X (2010).
19. Gibson, S. R. et al. Keck Planet Finder: design updates. *Proc. SPIE* **11447**, 1144742 (2020).
20. Stürmer, J. et al. A rubidium traced white-light etalon calibrator for MAROON-X. *Proc. SPIE* **9912**, 991229 (2016).
21. Schwab, C. et al. Design of NEID, an extreme precision Doppler spectrograph for WIYN. *Proc. SPIE* **9908**, 99087H (2016).
22. Grieves, N. et al. NIRPS: the Near-InfraRed Planet Searcher joining HARPS on the 3.6-m. In *European Planetary Science Congress 2021* EPSC2021-555 (Europlanet Science Congress, 2021).
23. Cersullo, F., Wildi, François, Chazelas, B. & Pepe, F. A new infrared Fabry-Pérot-based radial-velocity-reference module for the spirou radial-velocity spectrograph. *Astron. Astrophys.* **601**, A102 (2017).
24. Crepp, J. R. et al. iLocater: a diffraction-limited Doppler spectrometer for the Large Binocular Telescope. *Proc. SPIE* **9908**, 990819 (2016).
25. Szentgyorgyi, A. et al. G@M: design of the Giant Magellan Telescope Consortium Large Earth Finder (G-CLEF) for operations at the Magellan telescopes. *Proc. SPIE* **12184**, 121841N (SPIE, 2022).
26. Martin, M. J. & Ye, J. in *Optical Coatings and Thermal Noise in Precision Measurement* (eds Harry, G. M. et al.) 237–258 (Cambridge University Press, 2012).
27. Storz, R., Braxmaier, C., Jäck, K., Pradl, O. & Schiller, S. Ultrahigh long-term dimensional stability of a sapphire cryogenic optical resonator. *Opt. Lett.* **23**, 1031–1033 (1998).
28. Robinson, J. M. et al. Crystalline optical cavity at 4 K with thermal-noise-limited instability and ultralow drift. *Optica* **6**, 240–243 (2019).
29. Alnis, J., Matveev, A., Kolachevsky, N., Udem, T. & Hänsch, T. W. Subhertz linewidth diode lasers by stabilization to vibrationally and thermally compensated ultralow-expansion glass Fabry-Pérot cavities. *Phys. Rev. A* **77**, 053809 (2008).

30. Hirata, S., Akatsuka, T., Ohtake, Y. & Morinaga, A. Sub-hertz-linewidth diode laser stabilized to an ultralow-drift high-finesse optical cavity. *Appl. Phys. Express* **7**, 022705 (2014).
31. Ito, I., Silva, A., Nakamura, T. & Kobayashi, Y. Stable CW laser based on low thermal expansion ceramic cavity with 4.9 mHz/s frequency drift. *Opt. Express* **25**, 26020–26028 (2017).
32. Schwab, C. et al. Stabilizing a Fabry-Pérot etalon peak to 3 cm s for spectrograph calibration. *Publ. Astron. Soc. Pacif.* **127**, 880–889 (2015).
33. Betters, C. H., Leon-Saval, S. G. & Bland-Hawthorn, J. Photonic comb: a stabilized single-mode fiber etalon for wavelength calibration. *Appl. Opt.* **63**, D14–D20 (2024).
34. Tang, L. et al. Drift performance and chromatic thermal response of a temperature stabilized solid-etalon calibrator. *Astron. J.* **165**, 156 (2023).
35. Berthold, J. W., Jacobs, S. F. & Norton, M. A. Dimensional stability of fused silica, invar, and several ultra-low thermal expansion materials. *Metrologia* **13**, 9–16 (1977).
36. Hils, D., Hall, J. L. & De Marchi, A. in *Frequency Standards and Metrology* (ed. De Marchi, A.) 162–173 (Springer, 1989).
37. Jennings, J. et al. Frequency stability of the mode spectrum of broad bandwidth Fabry-Pérot interferometers. *OSA Contin.* **3**, 1177–1193 (2020).
38. Hill, I. R. et al. Dual-axis cubic cavity for drift-compensated multi-wavelength laser stabilisation. *Opt. Express* **29**, 36758–36768 (2021).
39. Wang, S. et al. Integrated multiple wavelength stabilization on a multi-channel cavity for a transportable optical clock. *Opt. Express* **28**, 11852–11860 (2020).
40. Milani, G. et al. Multiple wavelength stabilization on a single optical cavity using the offset sideband locking technique. *Opt. Lett.* **42**, 1970–1973 (2017).
41. Arias, N., González, L. J., Abediyeh, V. & Gomez, E. Frequency locking of multiple lasers to an optical cavity. *J. Opt. Soc. Am. B* **35**, 2394–2398 (2018).
42. Dawel, F. et al. Coherent photo-thermal noise cancellation in a dual-wavelength optical cavity for narrow-linewidth laser frequency stabilisation. *Opt. Express* **32**, 7276–7288 (2024).
43. Berthold, J. *Dimensionality Stability of Low Expansion Materials – Time Dependent Changes in Optical Contact Interfaces and Phase Shifts on Reflection from Multilayer Dielectrics*. PhD thesis, Univ. Arizona (1976).
44. Kreider, M. K., Rehan, A. Q., Kent, R. M., Bezerra, A. T. & Rebello Sousa Dias, M. Al-Au thin films for thermally stable and highly sensitive plasmonic sensors. *J. Phys. Chem. C* **126**, 5628–5639 (2022).
45. Burnett, D. The relation between refractive index and density. *Math. Proc. Camb. Phil. Soc.* **23**, 907–911 (1927).
46. Abadias, G. & Guerin, P. In situ stress evolution during magnetron sputtering of transition metal nitride thin films. *Appl. Phys. Lett.* **93**, 111908 (2008).
47. Mahadevan, S. et al. The Habitable-zone Planet Finder: a status update on the development of a stabilized fiber-fed near-infrared spectrograph for the for the Hobby-Eberly telescope. *Proc. SPIE* **9147**, 91471G (2014).
48. Halverson, S. et al. A comprehensive radial velocity error budget for next generation Doppler spectrometers. *Proc. SPIE* 9908, 99086P (2016).
49. Robertson, P. et al. Ultrastable environment control for the NEID spectrometer: design and performance demonstration. *J. Astron. Telesc. Instrum. Syst.* **5**, 015003 (2019).
50. NEID Specsoft Team *NEID Data Reduction Pipeline: NEID-DRP* (NEID, 2024); https://neid.ipac.caltech.edu/docs/NEID-DRP
51. Kreider, M. K. et al. Quantifying broadband chromatic drifts in Fabry-Perot resonators for exoplanet science. *CU Scholar* https://scholar.colorado.edu/concern/datasets/m326m3334 (2024).

Acknowledgements

We acknowledge helpful discussions with J. Stürmer on mirror coatings, who has also pointed out the importance of relaxation of the stress in the outer dielectric coating layers and its impact on the variation of the mirror properties. We also acknowledge useful technical conversations with M. Rebello de Sousa Dias about optical modelling and material properties. We are grateful for financial support from NIST award number 70NANB18H006 from the US Department of Commerce (C.F.) and from NSF grant numbers AAG 2108512 (S.M.), ATI 2009889 (S.M.), ATI 2009982 (S.A.D.), ATI 2009955 (R.C.T.), AST 1310875 (S.A.D.) and AST 1310885 (S.M.). NEID DRP development is supported by JPL Subcontract 1644767 (C.F.B.). M.K.K. acknowledges support from the NSF Graduate Research Fellowship Program. The Hobby–Eberly Telescope (HET) is a joint project of the University of Texas at Austin, the Pennsylvania State University, Ludwig-Maximilians-Universität München and Georg-August-Universität Göttingen. The HET is named in honour of its principal benefactors, William P. Hobby and Robert E. Eberly. The Center for Exoplanets and Habitable Worlds and the Penn State Extraterrestrial Intelligence Center are supported by Penn State and its Eberly College of Science.

Author contributions

R.C.T., S.M., J.P.N., S.H., C.F.B., F.H., J.R., A.R., C.S. and J.T.W. built the NEID and HPF instruments and acquired the etalon drift data. M.K.K., C.F. and S.A.D. developed the model to explain the etalon drift. M.K.K., C.F., S.A.D., R.C.T. and S.M. analysed the data and wrote the initial draft of the paper. D.M. provided information on the mirror coating structure and advised on drift sources. All authors discussed the results and contributed to revising and editing the final paper.

Competing interests

The authors declare no competing interests.

Additional information

Supplementary information The online version contains supplementary material available at https://doi.org/10.1038/s41550-025-02486-x.

Correspondence and requests for materials should be addressed to Molly Kate Kreider or Scott A. Diddams.

Peer review information *Nature Astronomy* thanks Alexandre Cabral and Fei Zhao for their contribution to the peer review of this work.

Reprints and permissions information is available at www.nature.com/reprints.

Publisher's note Springer Nature remains neutral with regard to jurisdictional claims in published maps and institutional affiliations.

Springer Nature or its licensor (e.g. a society or other partner) holds exclusive rights to this article under a publishing agreement with the author(s) or other rightsholder(s); author self-archiving of the accepted manuscript version of this article is solely governed by the terms of such publishing agreement and applicable law.

© The Author(s), under exclusive licence to Springer Nature Limited 2025

[1]Department of Physics, University of Colorado Boulder, Boulder, CO, USA. [2]Electrical Computer and Energy Engineering, University of Colorado Boulder, Boulder, CO, USA. [3]Time and Frequency Division, National Institute of Standards and Technology, Boulder, CO, USA. [4]Department of Physics and Astronomy, Carleton College, Northfield, MN, USA. [5]Department of Astronomy & Astrophysics, The Pennsylvania State University, University Park, PA, USA. [6]Astrobiology Research Center, The Pennsylvania State University, University Park, PA, USA. [7]Center for Exoplanets and Habitable Worlds, The Pennsylvania State University, University Park, PA, USA. [8]Department of Astronomy and Astrophysics, Tata Institute of Fundamental Research, Mumbai, India. [9]Jet Propulsion Laboratory, California Institute of Technology, Pasadena, CA, USA. [10]Steward Observatory, University of Arizona, Tucson, AZ, USA. [11]LightMachinery Inc., Nepean, Ontario, Canada. [12]NSF NOIRLab, Tucson, AZ, USA. [13]Schmidt Sciences, New York, NY, USA. [14]School of Mathematical and Physical Sciences, Macquarie University, North Ryde, New South Wales, Australia. [15]Penn State Extraterrestrial Intelligence Center, University Park, PA, USA. ✉e-mail: mollykate.kreider@colorado.edu; scott.diddams@colorado.edu